JOURNAL OF APPLIED PHYSICS **117**, 125301 (2015)

Femtosecond-laser hyperdoping silicon in an SF_6 atmosphere: Dopant incorporation mechanism

Meng-Ju Sher,[1,a)] Niall M. Mangan,[2] Matthew J. Smith,[3] Yu-Ting Lin,[2] Sophie Marbach,[2,4] Tobias M. Schneider,[2,5] Silvija Gradečak,[3] Michael P. Brenner,[2] and Eric Mazur[1,2]
[1]*Department of Physics, Harvard University, Cambridge, Massachusetts 02138, USA*
[2]*School of Engineering and Applied Sciences, Harvard University, Cambridge, Massachusetts 02138, USA*
[3]*Department of Materials Science and Engineering, Massachusetts Institute of Technology, Cambridge, Massachusetts 02139, USA*
[4]*ICFP, Department of Physics, Ecole Normale Superieure, Paris 75005, France*
[5]*Emergent Complexity in Physical Systems Laboratory (ECPS), Ecole Polytechnique Fédérale de Lausanne, Station 9, CH-1015, Switzerland*

(Received 17 December 2014; accepted 28 February 2015; published online 24 March 2015)

In this paper, we examine the fundamental processes that occur during femtosecond-laser hyperdoping of silicon with a gas-phase dopant precursor. We probe the dopant concentration profile as a function of the number of laser pulses and pressure of the dopant precursor (sulfur hexafluoride). In contrast to previous studies, we show the hyperdoped layer is single crystalline. From the dose dependence on pressure, we conclude that surface adsorbed molecules are the dominant source of the dopant atoms. Using numerical simulation, we estimate the change in flux with increasing number of laser pulses to fit the concentration profiles. We hypothesize that the native oxide plays an important role in setting the surface boundary condition. As a result of the removal of the native oxide by successive laser pulses, dopant incorporation is more efficient during the later stage of laser irradiation. © *2015 AIP Publishing LLC*. [http://dx.doi.org/10.1063/1.4914520]

I. INTRODUCTION

Using pulsed lasers to introduce non-equilibrium concentrations of dopants into silicon (Si), also called hyperdoping, is a promising technique for fabricating Si with unique properties. For example, Si becomes a superconductor when hyperdoped with boron to greater than 5 at. %.[1] When heavy chalcogens (S, Se, or Te) are incorporated in Si at concentrations near 1 at. %, the hyperdoped Si exhibits infrared absorption as well as photocurrent response at photon energies below the band-gap energy of Si.[2–5] Moreover, hyperdoping with ultrafast lasers can cause laser-induced periodic surface structures (LIPSS) that act as light trapping structures.[6,7] Hyperdoping using femtosecond (fs) lasers, however, often results in poor material crystallinity, and there is no reliable method for controlling the concentration profile.[8]

The key processes during pulsed-laser hyperdoping are shown in Figure 1. After laser irradiation, the dopant atoms diffuse in from the surface while the silicon is molten. If the dopant concentration in the liquid is higher than the maximum solubility in the solid, the resolidification dynamics determines the amount of dopant (solute) incorporated (trapped) into the solid phase. Solute trapping depends on the resolidification velocity and the diffusive velocity of the dopant.[9,10] If the resolidification interface velocity is smaller than the diffusive velocity of the dopant atoms, excess dopant atoms are rejected into the melt from the solid. If the resolidification velocity is larger than the diffusive velocity, solute trapping occurs, yielding a dopant concentration higher than thermodynamically favorable.[10,11] While solute trapping has been studied extensively,[12,13] the dopant incorporation mechanism (i.e., how the dopant at the surface diffuses into the melt) and the resulting dopant concentration profile are not well characterized.[14]

This paper focuses on understanding the hyperdoping of sulfur in silicon using fs-laser pulses using a gas-phase dopant precursor. For S hyperdoping, sulfur hexafluoride (SF_6), a stable and inert gas, is an ideal dopant precursor. However, as the equilibrium S concentration in Si is low (maximum $3 \times 10^{16}\,cm^{-3}$),[15] solute trapping is necessary to achieve the concentration at which interesting optoelectronic properties are reported. We perform hyperdoping using fs-laser pulses at a fluence of $2.5\,kJ/m^2$ which results in a crystalline hyperdoped layer. We study how the pressure of the dopant precursor and the number of laser pulses influence the dopant concentration profile. This work provides insight into the dopant incorporation mechanism and fabrication guidelines for fs-laser hyperdoping of Si.

II. EXPERIMENTAL

To achieve hyperdoping, we use an amplified Ti:sapphire fs-laser system (80-fs pulse duration, 800-nm center wavelength, and 100-Hz repetition rate) and focus the laser spot to a diameter of 460 μm (full-width-half-maximum of Gaussian beam profile). We first performed laser irradiation tests on Si to identify the processing parameters that produce samples suitable for concentration measurements. To measure the dopant concentration profiles accurately, the surface of the samples needs to be flat and free of laser-

a)Present address: Materials Science and Engineering Stanford University, Stanford, California 94305, USA. Electronic mail: msher@stanford.edu

 © 2015 AIP Publishing LLC

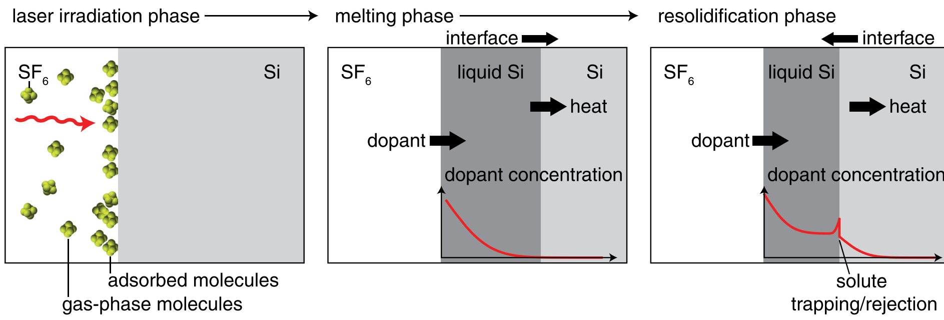

FIG. 1. Schematics of the dopant diffusion process during pulsed-laser melting and resolidification. For clarity, SF_6 molecules are only illustrated in the left panel. The arrows show the influx of dopant, heat diffusion, and solid-liquid interface movement. The red curves in the middle and right panels are illustrations of the dopant diffusion profile and effect of solute trapping/rejection.

ablated particles. After examining the surface of Si samples irradiated with 1–10 laser pulses at fluences between 2.0 and 4.0 kJ/m^2, we determined that irradiation with six laser pulses at 2.5 kJ/m^2 produced samples with a flat surface, with no evidence of LIPSS nor any ablated particles.

To examine the microstructure of the hyperdoped Si, we performed Raman spectroscopy to detect the presence of amorphous Si phases by monitoring the signature amorphous Si modes at 150 cm^{-1} and 480 cm^{-1}. We used a Raman spectrometer with a 10-mW, 632.8-nm HeNe laser, recorded through a 20× objective with a spot size of approximately 10 μm. To support our Raman measurements, we also investigated the microstructure of one sample with transmission electron microscopy (TEM). Cross-sectional TEM samples were prepared using the lift-out method on a dual-beam focused ion beam. Bright-field TEM images were collected with a transmission electron microscope operated at 200 kV.

For hyperdoping, the samples are irradiated with one to six laser pulses with a laser fluence of 2.5 kJ/m^2 at an SF_6 pressure ranging from vacuum (10^{-6} Torr) to 500 Torr. Prior to laser treatment, Si wafers (float-zone grown, p-type, 3 kΩ cm) are solvent-cleaned and etched with alignment markers using standard photolithography and reactive ion-etching recipes. The alignment markers are mesas 800 μm in diameter and 1.5 μm in height. We then place the sample in a vacuum chamber, pump down to 10^{-6} Torr, and fill the chamber with SF_6 to the desired pressure.

To characterize the dopant concentration as a function of depth, we perform secondary ion mass spectrometry (SIMS) measurements. The SIMS measurements are carried out using a 6-keV Cs ion beam with a current of 4 nA. We perform SIMS measurements on a region of $20 \times 30\ \mu m^2$ at the center of the laser irradiated spot. The area probed is small compared to the laser spot size (460-μm diameter) to minimize the spatial variation of the local laser fluence across the SIMS sample region (<1%). We record counts of ^{29}Si, ^{32}S, ^{34}S, ^{19}F, and ^{18}O, and the S and F counts are calibrated against known ion-implanted Si samples.

III. RESULTS

We first study the microstructure of a sample after laser irradiation at a fluence of 2.5 kJ/m^2. Figure 2(a) shows Raman spectra normalized to the strong crystalline Si signal at 520 cm^{-1}, demonstrating that the center of the laser irradiated area is crystalline. The optical microscope image of the sample in the inset in Figure 2(a) shows a ring with visible color contrast (the laser beam diameter is larger than the field of view). The Raman spectrum from this ring confirms that it is amorphous. Figure 2(b) shows a cross-sectional TEM image at the center of the laser irradiated spot. Fast Fourier transform of the TEM image from the square area in Figure 2(b) shows that the center of the sample is single crystalline (Figure 2(b) inset).

The SIMS measurements in Figure 3 show the dependence of S concentration on SF_6 pressure P and the number of

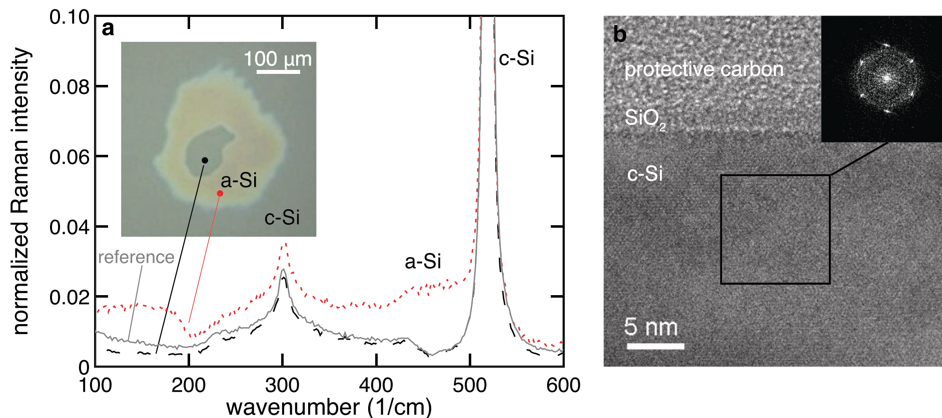

FIG. 2. Microstructure of a sample hyperdoped at 100 Torr SF_6 with four laser pulses. (a) Raman spectra taken from three different locations of the sample: the center (black dashed line), edge of the laser irradiated spot (red dotted line), and a reference Si without laser irradiation (gray solid line). The locations are marked in the optical microscope image in the inset. (b) Bright-field TEM image taken from the center of the laser-irradiated spot. The labels indicate protective carbon layer, native surface oxide SiO_2, and the hyperdoped area, c-Si. Inset: Fast Fourier transform of the TEM image from a hyperdoped area indicated in (b) shows the center of the laser-irradiated region is single crystalline.

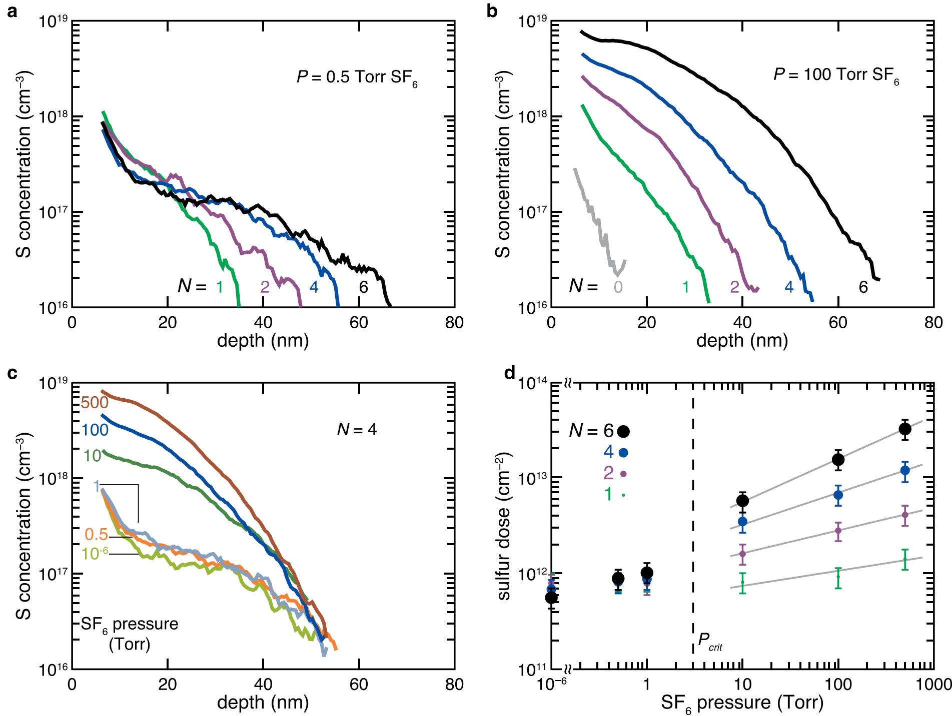

FIG. 3. Sulfur concentration profiles of samples hyperdoped at (a) 0.5 Torr and (b) 100 Torr. Sulfur concentration of a Si control sample (labeled $N = 0$) is also shown. (c) Sulfur concentration profiles of samples irradiated by four laser pulses at different pressures. (d) Total incorporated S dose, D, as a function of SF_6 pressure, P, and number of laser pulses, N. The lines represent the slopes, β, of data points between 1 and 500 Torr. $D \propto P^{\beta}$. $\beta = 0.16$, 0.24, 0.33, and 0.45 for $N = 1$, 2, 4, and 6, respectively. All observed values of β are smaller than 1.

laser pulses N. Figure 3(a) shows S concentration profiles of samples irradiated at 0.5 Torr. At this pressure, dopants are incorporated deeper into Si with each additional laser pulse, but the total S dose (area under the concentration curve) remains constant. At a pressure of 100 Torr, on the other hand, both the surface concentration and the depth of the dopant distribution increase with the number of laser pulses (Figure 3(b)). In all profiles, the sulfur concentration exceeds the maximum solubility of S in solid Si ($3 \times 10^{16}\,\mathrm{cm}^{-3}$).

The S count of the Si control sample without laser irradiation ($N = 0$ curve in Figure 3(b)) shows a small decreasing signal that extends to a depth of 10 nm. This curve reveals two uncertainties of our measurements: (1) a small contribution from oxygen signal and (2) the depth resolution. Because ionized O_2 has the same mass as S, the presence of a native oxide contributes to the total count in the mass spectrometer.[8] For the hyperdoped samples, the error from ionized oxygen molecules is a small percentage of the S count (<10%). Secondly, the Cs ion milling drives a portion of the atoms from the surface further into the sample; the $N = 0$ control sample measurement in Figure 3(b) suggests a resulting depth measurement uncertainty of about 10 nm.[16]

To directly compare the dopant concentration profiles at different pressures, Figure 3(c) shows samples irradiated by four laser pulses across the entire range of pressures investigated. For samples hyperdoped at or below 1 Torr, the concentration profiles are identical. For P greater or equal to 10 Torr, the S concentration at the surface increases with pressure. Regardless of the SF_6 pressure, the dopant incorporation depth is the same.

We show in Figure 3(d) the total incorporated S dose (number of S atom per unit area). Because SIMS cannot accurately measure the dopant concentration near the surface (within 5 nm), the dose reported here is a lower bound on the total incorporated S. The figure shows two pressure regimes, with a transition at some critical pressure, P_{crit}, between 1 and 10 Torr. At SF_6 pressures smaller than P_{crit}, the S dose is independent of pressure and of the number of laser pulses. At pressures greater than P_{crit}, the S dose increases with both pressure and number of laser pulses.

We also recorded fluorine concentration and found that F atoms are also incorporated into Si (data not shown). The F concentration profiles have the same shape as S concentration profiles and the incorporation depth is also the same. The F dose is about two times the S dose.

IV. DISCUSSION

A. Crystalline phase

The laser fluence used in this paper is carefully chosen so as to optimize the material crystallinity and minimize surface texturing. Unlike previous studies where we used fluences above the ablation threshold and produced amorphous material,[8] in this paper, we use a lower fluence of 2.5 kJ/m^2 and observe a crystalline phase (Figure 2). Bonse *et al.* report that there is a small fluence range between the melting and ablation threshold where the laser treated material is crystalline.[17] For Si, a crystalline phase cannot form if the resolidification process is fast; if the solid-liquid interface moves faster than 15 m/s, the resolidified Si is amorphous.[18] Therefore, we can identify 15 m/s as an upper bound of the interface velocity during the entire resolidification process.

Although we identified a fluence where the hyperdoped Si is crystalline, the outer edge of the laser-treated spot is amorphous. Because of the Gaussian laser intensity profile, the fluence at the edges of the irradiated area is lower, and the resolidification velocity is different. Gimpel *et al.* show that the amorphous phase is also enhanced when scanning the laser pulses, as is commonly done when fabricating

large-area hyperdoped Si.[19] For large area fabrication, the amorphous region could be minimized using a flat-top beam.

B. Source of dopant atoms

There are two possible sources of dopant precursors: molecules adsorbed on the Si surface prior to laser irradiation and gas-phase molecules impinging on the molten Si surface (Figure 1).[20] The number of gas-phase molecules impinging on the Si surface is linearly proportional to the pressure, while the thickness of the adsorbed layer of molecules depends on the adsorption isotherm and can be a nonlinear function of pressure. We can determine the type of dopant precursors (adsorbed or gas-phase) by examining how the dopant incorporation depends on pressure.

In the low-pressure regime ($<P_{crit}$), the rate of gas phase molecules impinging on the molten Si surface is not high enough to account for the dopant incorporation. From the ideal gas law, it follows that the impingement rate of SF_6 molecules on a surface is $1 \times 10^{20}\,cm^{-2}s^{-1}$ at 0.5 Torr (Table I).[21] We also know that the silicon resolidifies within 8 ns,[8] implying that the impingement flux of gas phase molecule on the molten silicon is $8 \times 10^{11}\,cm^{-2}$. Below P_{crit}, the S dose is on the order of $10^{12}\,cm^{-2}$, so to achieve the observed S dose from gas phase molecules, all the molecules striking the Si surface need to be incorporated, which is unlikely. Furthermore, in vacuum, where the impingement rate of molecules is six orders of magnitude smaller, we observe the same S dose of $10^{12}\,cm^{-2}$. Therefore, below P_{crit}, the gas phase SF_6 molecules are not sufficient to account for the amount of S incorporated. Both the pressure independence of S incorporation below P_{crit} and the high level of doping compared with the expected rate of S impingement indicate that the majority of the dopant must come from a layer of SF_6 molecules adsorbed on the Si surface.

In the high-pressure regime ($>P_{crit}$), S incorporation increases with pressure; the pressure dependence is a power law, $D \propto P^{\beta}$ with $\beta < 1$. Because the impingement rate of SF_6 molecules increases linearly with pressure (which would result in $\beta = 1$), a $\beta < 1$ suggests that gas phase molecules are not the dominant source in this pressure regime either. The dependence of the adsorbed layer thickness on pressure is likely to result in the observed non-linear pressure dependence of the S dose.[22,23] In summary, surface adsorbed SF_6 molecules are likely to be the main dopant source in both pressure regimes.

TABLE I. Impingement rate J_{imp} of SF_6 molecules at different pressures. The impingement rate is given by $J_{imp} = N_A P/\sqrt{2\pi MRT}$, where N_A is Avogadro's number, P is the pressure, $M = 146$ g/mol is the molecular weight of SF_6, R is the universal gas constant, and T is temperature.[21] Based on the impingement rate and assuming a surface density of $10^{15}\,cm^{-2}$, we calculate the minimum time it takes to build up monolayer coverage by assuming the sticking coefficient is equal to 1 (all molecules impinging on the surface stay on the surface). The last two columns show measured S dose after 1 and 6 laser pulses.

P (Torr)	J_{imp} ($cm^{-2}\,s^{-1}$)	Minimum time to build up a monolayer	S dose $N = 1$ ($10^{12}\,cm^{-2}$)	S dose $N = 6$ ($10^{12}\,cm^{-2}$)
10^{-6}	2×10^{14}	5 s	0.8 ± 0.2	0.6 ± 0.1
0.5	1×10^{20}	10 μs	0.8 ± 0.2	0.9 ± 0.2
1	2×10^{20}	5 μs	0.9 ± 0.2	1.1 ± 0.3
10	2×10^{21}	0.5 μs	0.8 ± 0.2	5.9 ± 1.4
100	2×10^{22}	50 ns	0.9 ± 0.2	15.8 ± 3.7
500	1×10^{23}	10 ns	1.4 ± 0.3	33.0 ± 7.8

Previous studies on hyperdoping Si using SF_6 as dopant precursors do not focus on F incorporation,[24] but our measurements reveal a significant amount of F incorporation. When SF_6 molecules are excited or ionized, they can react with Si and create silicon tetrafluoride (SiF_4) which is volatile and is not incorporated into silicon.[25,26,28] We hypothesize instead that after laser melting, the SF_6 molecules thermally decompose at the gas-liquid interface. Part of the F atoms reacts with silicon, and part is incorporated into silicon.[27] As a result, both S and F are incorporated, and we observe a F concentration about twice that of S. The structural and electronic properties of F dopant in Si are not well known, although some reports suggest F atoms form small SiF_4 clusters inside crystalline Si.[29,30]

C. Pulse number dependence and dopant incorporation mechanism

In this section, we discuss the native oxide on the surface and its possible role as a diffusion barrier. First we show the amount of dopant incorporated is only a small fraction of the adsorbed dopant molecules. To emphasize that equilibrium adsorption is achieved before the laser irradiation, Table I shows the minimum time required for a monolayer of SF_6 molecules to build up on a Si surface if the sticking coefficient is unity. At 10^{-6} Torr, it takes only on the order of 5 s for SF_6 molecules to accumulate a monolayer on the Si surface, much shorter than the time scale required for setting up the experiment. The time required for accumulating a monolayer is orders of magnitude smaller at higher pressures. Therefore, the amount of SF_6 molecules adsorbed on the surface of Si should be at equilibrium before the hyperdoping process. After one laser pulse, the S dose ($10^{12}\,cm^{-2}$) is orders of magnitude smaller than the density of S atoms in a monolayer of surface coverage ($10^{15}\,cm^{-2}$, see Figure 3(d)). This suggests that only a fraction of the adsorbed dopant molecules is incorporated during the hyperdoping process. We propose that the native oxide layer acts as a diffusion barrier, limiting S incorporation following fs-laser irradiation.

Further evidence for the role of the native oxide as a diffusion barrier can be obtained by examining changes in S dose with increasing number of laser pulses N. At pressures equal to 100 and 500 Torr, the S dose increases more than linearly with respect to the number of laser pulses. Table I shows that at 100 Torr, the S dose increases 18 times between $N = 1$ and $N = 6$; and similarly at 500 Torr, the S dose increases 24 times. Possible mechanisms for increased incorporation are that the native oxide on the surface is removed by subsequent laser pulses[31] or etched away by ionized SF_6.[32] Without the surface oxide,[23] S atoms can diffuse into Si more easily and increase S incorporation from the surface.

Changes to the oxide layer after multiple laser pulses could explain not only the increase in dose, but also

variations in concentration profile shape. The adsorbed dopant molecules can enter molten silicon in one (or a combination) of two ways: (1) the molecules enter relatively slowly (as a flux) over the entire duration of the melting and the solidification phase, (2) the total dose of dopant molecules enter immediately upon melting. We will refer to mechanism 1 as a "surface flux" and mechanism 2 as an "instant dose." An outward flux of sulfur has been observed during ns-laser processing of ion implanted silicon. This outward flux is found to depend on the presence of a native oxide layer.[13] We hypothesize that in our system, the native oxide layer acts as a diffusion barrier. When there is native oxide on the surface, S enters the molten Si as a surface flux. After the oxide layer is removed by successive laser pulses, there is no diffusion barrier and the adsorbed dopant precursor is immediately incorporated into the Si as an instant dose. For an intermediate range of native oxide layer thicknesses, we can model the S incorporation as a combination of instant dose and continuous surface flux.

We numerically simulate simultaneously both the melting and solute dynamics to obtain the dopant concentration profile (Supplemental Material[33]). We use established models for nanosecond-laser melting,[12,13,34,35] adjusted to account for femtosecond laser energy absorption, rapid thermalization, and slow thermal melting.[36] We simulate thermal melting with a melt depth of 60 nm and solidification velocity of 12.5 m/s. We treat the diffusion and incorporation of S into Si using a continuous non-equilibrium growth model.[34] Surface flux and instant dose represent different boundary conditions at the surface. For a given total S dose from experimental data (Figure 3(d)), we simulate material incorporated entirely from surface flux and entirely from instant dose and then linearly combine the two resulting profiles, fitting the relative contribution from each boundary condition. The profiles may be linearly combined because diffusion, constant flux, and instant dose are all inherently linear (Supplemental Figure S1 (Ref. 33)). Further discussion of simulation and fitting can be found in Ref. 37.

Figure 4 shows that our fitted simulation results closely match the experimental data. In the measured concentration profiles of Si hyperdoped at 500 Torr, the shape of the dopant profile changes as the number of laser pulses is increased from 1 to 6 laser pulses. The profiles for $N \leq 2$ appear exponential, while those for $N \geq 4$ have a plateau between a depth of 10 and 20 nm. Figure 4 inset shows that a monotonic change in the boundary condition from primarily surface flux to primarily instant dose best fits the experimental data. The main effect of the change in the boundary condition is an increase in effective diffusion time. This observation suggests that as the native oxide layer depletes, a larger proportion of the dose diffuses into the silicon right after it melts. Sulfur incorporated as an instant dose has more time to diffuse and equilibrate across the region, forming the plateau observed in profiles for $N = 4$ and 6. These results support our hypothesis that the oxide diffusion barrier changes as the number of laser pulses is increased. Our study suggests that the dopant profile can be engineered by manipulating the surface oxide layer, thereby controlling the dopant incorporation mechanism.

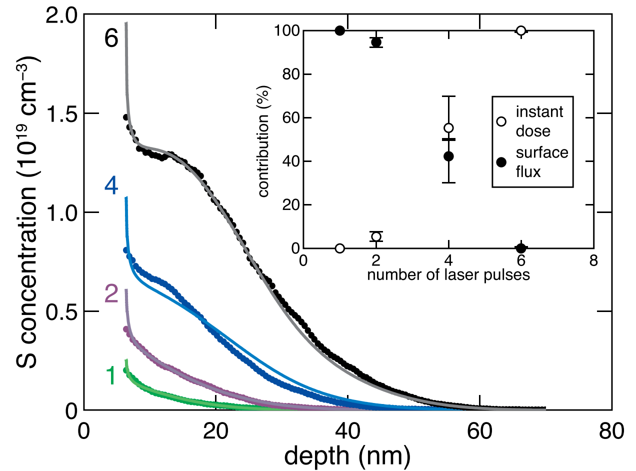

FIG. 4. Comparison between S concentration profiles (dots) and simulation results (solid lines) for $P = 500$ Torr. Profile shapes are exponential for $N \leq 2$. For $N \geq 4$, a plateau forms at a depth between 10 and 20 nm. Numerical simulation results are fit to concentration profiles by determining the total dose from experiment and fitting the relative contributions from instant dose and surface flux as described in the text. The inset shows the contributions from instant dose (open circles) and surface flux (filled circles) as a function of the number of laser pulses. Error bars on the proportion of instant dose and surface flux reflect 95% confidence intervals in the fit for $N = 1$ and 2. Error bars for $N = 4$ reflect the possible range of total dose for $N = 3$ (from the dose incorporated during $N = 2$ to the half the dose incorporated between $N = 2$ and 4), and range of incorporation mechanism (from 0 to 100% flux). A similar analysis was done for error on the $N = 6$.

V. CONCLUSION

We performed fs-laser hyperdoping under different dopant precursor pressures with varying number of laser pulses and achieve single crystalline hyperdoped Si at a fluence of 2.5 kJ/m^2. By measuring the resultant dopant profile using SIMS, we identified two pressure regimes. At pressures below 1 Torr, the dose of S is independent of pressure and the number of laser pulses; at pressures above 10 Torr, the S dose increases with both pressure and the number of laser pulses. Analyzing the pressure dependence of dopant incorporation reveals that the surface adsorbed molecules are the dominant source of the dopant material. Analyzing the effect of multiple pulse irradiation shows that the dopant incorporation depth and profile can be controlled by the number of laser pulses. We also show that the native surface oxide layer forms a diffusion barrier that limits dopant incorporation. Numerical simulation reveals that without a diffusion barrier at the surface, dopant is incorporated more efficiently and the concentration profile has a plateau. Our results provide new insights into the dopant incorporation mechanism, fabrication guidelines for hyperdoping Si with high crystalline quality, and a model for predicting dopant concentration profiles.

ACKNOWLEDGMENTS

M.-J. S. fabricated the samples, and carried out SIMS measurements. Y.-T.L. acquired the Raman data, and M.J.S (supervised by S.G.) prepared the TEM images. N.M., S.M., and T.M.S. performed numerical modeling. E.M. and M.P.B supervised the research. The authors are indebted to Dr. Tom

Mates (UCSB), Professor Michael Aziz, and Professor Robert Madix for valuable discussions. The research described in this paper was supported by the Chesonis Family Foundation and the National Science Foundation under Contract Nos. DMR-0934480 and EEC-1041895. M.P.B is an investigator of the Simons Foundation. This work was performed in part at the Center for Nanoscale Systems (CNS) supported by NSF Award No. ECS-0335765 and in part at the UCSB MRSEC supported by NSF Award No. DMR-1121053.

[1]E. Bustarret, C. Marcenat, P. Achatz, J. Kacmarcik, F. Levy, A. Huxley, L. Ortega, E. Bourgeois, X. Blase, D. Debarre, and J. Boulmer, Nature **444**, 465 (2006).
[2]S. H. Pan, D. Recht, S. Charnvanichborikarn, J. S. Williams, and M. J. Aziz, Appl. Phys. Lett. **98**, 121913 (2011).
[3]M.-J. Sher, Y.-T. Lin, M. T. Winkler, E. Mazur, C. Pruner, and A. Asenbaum, J. Appl. Phys. **113**, 063520 (2013).
[4]S. X. Hu, P. D. Han, S. Wang, X. Mao, X. Y. Li, and L. P. Gao, Semicond. Sci. Technol. **27**, 102002 (2012).
[5]J. E. Carey, C. H. Crouch, M. Y. Shen, and E. Mazur, Opt. Lett. **30**, 1773 (2005).
[6]T. Sarnet, J. E. Carey, and E. Mazur, AIP Conf. Proc. **1464**, 219 (2012).
[7]M.-J. Sher, M. T. Winkler, and E. Mazur, MRS Bull. **36**, 439 (2011).
[8]M. T. Winkler, M.-J. Sher, Y.-T. Lin, M. J. Smith, H. Zhang, S. Gradecak, and E. Mazur, J. Appl. Phys. **111**, 093511 (2012).
[9]C. W. White, S. R. Wilson, B. R. Appleton, and F. W. Young, J. Appl. Phys. **51**, 738 (1980).
[10]R. Reitano, P. M. Smith, and M. J. Aziz, J. Appl. Phys. **76**, 1518 (1994).
[11]J. A. Kittl, P. G. Sanders, M. J. Aziz, D. P. Brunco, and M. O. Thompson, Acta Mater. **48**, 4797 (2000).
[12]B. P. Bob, A. Kohno, S. Charnvanichborikarn, J. M. Warrender, I. Umezu, M. Tabbal, J. S. Williams, and M. J. Aziz, J. Appl. Phys. **107**, 123506 (2010).
[13]D. Recht, J. T. Sullivan, R. Reedy, T. Buonassisi, and M. J. Aziz, Appl. Phys. Lett. **100**, 112112 (2012).
[14]E. Landi, P. G. Carey, and T. W. Sigmon, IEEE Trans. Comput.-Aided Des. **7**, 205 (1988).
[15]R. O. Carlson, R. N. Hall, and E. M. Pell, J. Phys. Chem. Solids **8**, 81 (1959).
[16]K. Wittmaack, Vacuum **34**, 119 (1984).
[17]J. Bonse, S. Baudach, J. Kruger, W. Kautek, and M. Lenzner, Appl. Phys. A: Mater. Sci. Process. **74**, 19 (2002).
[18]M. O. Thompson, J. W. Mayer, A. G. Cullis, H. C. Webber, N. G. Chew, J. M. Poate, and D. C. Jacobson, Phys. Rev. Lett. **50**, 896 (1983).
[19]T. Gimpel, I. Hoger, F. Falk, W. Schade, and S. Kontermann, Appl. Phys. Lett. **101**, 111911 (2012).
[20]A. Slaoui, F. Foulon, R. Stuck, and P. Siffert, Appl. Phys. A: Mater. Sci. Process. **50**, 479 (1990).
[21]G. A. Somorjai, *Introduction to Surface Chemistry and Catalysis* (Wiley, New York, 1993), p. 12.
[22]A. Slaoui, F. Foulon, and P. Siffert, J. Appl. Phys. **67**, 6197 (1990).
[23]G. G. Bentini, M. Bianconi, L. Correra, R. Nipoti, D. A. Patti, and A. Gasparotto, Appl. Surf. Sci. **36**, 394 (1989).
[24]C. H. Crouch, J. E. Carey, M. Shen, E. Mazur, and F. Y, Genin, Appl. Phys. A: Mater. Sci. Process. **79**, 1635 (2004).
[25]T. J. Chuang, J. Chem. Phys. **74**, 1453 (1981).
[26]J. Royer, P. Y. Tessier, B. Grolleau, and G. Turban, J. Vac. Sci. Technol. A **14**, 234 (1996).
[27]It has been reported that SF_6 molecules dissociate under intense laser irradiation at 800 nm but this phenomenon is only observed at intensities more than two orders of magnitude higher than the process used in this experiment.[28]
[28]J. H. Sanderson, R. V. Thomas, W. A. Bryan, W. R. Newell, P. F. Taday, and A. Langley, J. Phys. B: At., Mol. Opt. Phys. **30**, 4499 (1997).
[29]D. De Salvador, G. Bisognin, E. Napolitani, M. Mastromatteo, N. Baggio, A. Carnera, F. Boscherini, G. Impellizzeri, S. Mirabella, S. Boninelli, F. Priolo, and F. Cristiano, Appl. Phys. Lett. **95**, 101908 (2009).
[30]F. Panciera, K. Hoummada, M. Mastromatteo, D. De Salvador, E. Napolitani, S. Boninelli, G. Impellizzeri, F. Priolo, A. Carnera, and D. Mangelinck, Appl. Phys. Lett. **101**, 103113 (2012).
[31]Z. L. Wang, J. F. M. Westendorp, and F. W. Saris, Nucl. Instrum. Methods Phys. Res. **211**, 193 (1983).
[32]K. R. Williams, K. Gupta, and M. Wasilik, J. Microelectromech. Syst. **12**, 761 (2003).
[33]See supplementary material at http://dx.doi.org/10.1063/1.4914520 for the mathematical model and fitting methodology used to estimate the method of dopant incorporation.
[34]M. J. Aziz and T. Kaplan, Acta Metall. **36**, 2335 (1988).
[35]D. E. Hoglund, M. O. Thompson, and M. J. Aziz, Phys. Rev. B **58**, 189 (1998).
[36]D. P. Korfiatis, K. A. T. Thoma, and J. C. Vardaxoglou, J. Phys. D: Appl. Phys. **40**, 6803 (2007).
[37]N. M. Mangan, T. M. Schneider, S. Marbach, M.-J. Sher, Y.-T. Lin, E. Mazur, M. J. Aziz, and M. P. Brenner, “A model of the melting and solute dynamics of hyperdoping with a femtosecond laser” (unpublished); N. M. Mangan, “Organization and diffusion in biological and material fabrication problems,” Ph.D. dissertation (Harvard University, 2013).

Journal of Applied Physics is copyrighted by AIP Publishing LLC (AIP). Reuse of AIP content is subject to the terms at: http://scitation.aip.org/termsconditions. For more information, see http://publishing.aip.org/authors/rights-and-permissions.